Noncontact Viscoelastic Measurement of Polymer Thin Films in a Liquid Medium Using Long-Needle Atomic Force Microscopy

Dongshi Guan,[†] Chloé Barraud,[‡] Elisabeth Charlaix,[‡] and Penger Tong*,[†]

[†]Department of Physics, Hong Kong University of Science and Technology, Clear Water Bay, Kowloon, Hong Kong
[‡]LIPHY, Université Grenoble Alpes, F-38000 Grenoble, France

S *Supporting Information*

ABSTRACT: We report the noncontact measurement of the viscoelastic property of polymer thin films in a liquid medium using frequency-modulation atomic force microscopy with a newly developed long-needle probe. The probe contains a long vertical glass fiber with one end adhered to a cantilever beam and the other end with a sharp tip placed near the liquid–film interface. The nanoscale flow generated by the resonant oscillation of the needle tip provides a precise hydrodynamic force acting on the soft surface of the thin film. By accurately measuring the mechanical response of the thin film, we obtain the elastic and loss moduli of the thin film using the linear response theory of elastohydrodynamics. The experiment verifies the theory and demonstrates its applications. The technique can be used to accurately measure the viscoelastic property of soft surfaces, such as those made of polymers, nanobubbles, live cells, and tissues.
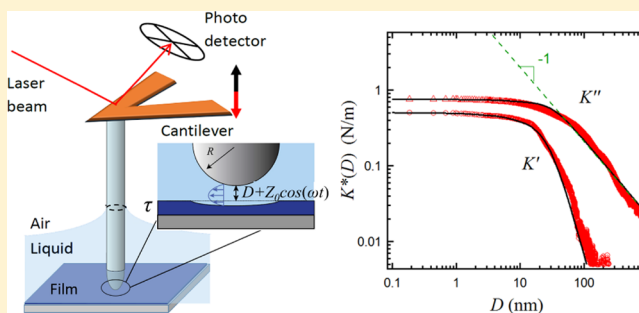
INTRODUCTION

Mechanical characterization of soft thin films in a liquid environment is of great interest for both scientific and industrial applications. In biology, for instance, direct measurement of the mechanical properties of a living cell is essential for the understanding of mechanisms by which cells sense physical stimuli and transduce them into biochemical signals that result in cellular responses.[1,2] It is also important to characterize the mechanical features of various extracellular media, such as collagen networks and polydimethylsiloxane (PDMS)-based biomaterials, which will in turn alter the cell structure and functions.[3] In surface science, the study of the mechanical properties of nanobubbles adsorbed at the liquid–solid interface plays an important role in understanding the stability and long lifetime of the nanobubbles.[4,5] In many industrial applications, there is a growing need for a rapid determination of the mechanical properties of thin polymer films and coatings.[6]

Many of the mechanical characterizations of thin films were conducted using the conventional contact mechanics methods,[7,8] which use a solid probe of a known shape, usually associated with either optical/magnetic tweezers or an atomic force microscope (AFM), to measure the force and contact area changes in the thin film under study when normal compression is imposed. However, the direct contact methods have limitations in determining the elastic modulus of very thin and soft materials, as these materials are often involved in adhesion with the probe, and it is quite difficult to accurately account for the amount of adhesion and contact region at an adhesive contact.[9,10] These materials are also vulnerable to

sample damage and probe contamination during measurement.[11]

A number of theoretical and numerical studies aimed at providing an alternative noncontact method for the mechanical characterization of soft materials via hydrodynamic interactions have been carried out.[12–14] Experimental attempts were also made to determine the mechanical properties of thin films in a viscous fluid.[15–18] So far, most of the nanomechanical devices were designed to operate in air or vacuum, and very few can function well in a liquid medium, as the significant viscous damping of the liquid diminishes their performance.[19–21] For example, when an AFM cantilever is immersed in a liquid, its motion is severely damped by the fluid viscosity so that its quality factor Q becomes very low ($Q \lesssim 5$).[22,23] The piezoelectric shaker, which drives the cantilever, also generates unwanted flow modes near the surface of the film under study, which in turn affects the operation of the AFM.

In this paper, we report a noncontact method to accurately measure the viscoelastic property of polymer thin films in a liquid medium. Using the frequency-modulation AFM (FM-AFM) with a newly developed long-needle probe, we find that the mechanical response of the thin film can be precisely measured via the oscillatory draining flow between the needle tip and the film surface. The elastic modulus and viscosity of the thin film are simultaneously obtained using the linear response theory of elastohydrodynamics (EHD). From the

measured viscoelasticity of ultrathin PDMS films with different values of film thickness (250−900 nm) and tip radius (800 and 220 nm), we verify the theory and demonstrate the applications of this new technique for the study of soft interfaces.

■ EXPERIMENTAL SECTION

Long-Needle Probe. To reduce the viscous damping on a conventional AFM cantilever when it is immersed in a liquid, we design a "long-needle" probe for FM-AFM working in a thin liquid layer. Figure 1 shows the working principle of the long-needle AFM
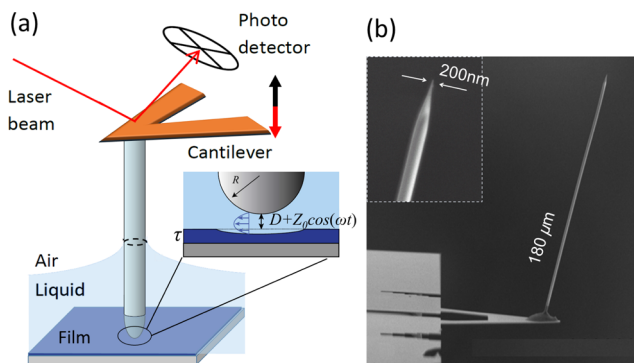

Figure 1. (a) Sketch of the long-needle AFM for the noncontact mechanical measurement of thin viscoelastic films in a liquid medium. (b) Scanning electron microscopy image of the actual long glass fiber of diameter $d \simeq 2.5$ μm and length $l \simeq 180$ μm. The inset shows a magnified image of the fiber tip with radius $R \simeq 200$ nm.

and the actual long glass needle probe. The probe contains a long vertical glass fiber with one end adhered to the front end of a cantilever beam and the other end immersed through a liquid−air interface. The glass fiber is pulled out of a capillary glass rod using a pipette puller, and its diameter d, length l, and tip radius R can all be programmed, respectively, to be in the ranges of 0.5−5 μm, 100−300 μm, and 50−1000 nm. The tip of the glass fiber is forged to be thinner and spherical.

The overall dimension of the long-needle probe is designed so that one can ignore the buoyancy force acting on the fiber, minimizing the effect of spatial averaging over the film surface, and facilitate the probe assembly, needle surface cleaning and treatment, and handling of liquid interfaces.[24,25] More details on the assembly of the long-needle probe are given in the Supporting Information. Because the major part of the cantilever probe is in air and only a small part of the fiber tip is in contact with the liquid, the entire cantilever system acts as a high-quality harmonic resonator with $Q \simeq 34$, which ensures that the long-needle AFM can function efficiently in a liquid environment.[26−28]

Thin-Film Preparation. The PDMS films under study are prepared using the spin-coating method on a float glass substrate (Pignat), which is cleaned before use by ultrasonication in ultrapure water and soap solution. The purchased PDMS (RTV 615, GE Silicones) and its curing agent are vigorously mixed in a 10:1 weight ratio and then degassed. To get a uniform film of thickness smaller than 1 μm, this viscous initial mixture is diluted with heptane to make a 3% PDMS solution for films of thicknesses 260 and 440 nm and a 7% PDMS solution for the film of thickness 888 nm. A 50 μL droplet of the solution is then spin-coated on the glass substrate for 1 min at a rotating speed of 1000 rpm for the 440 nm-thick sample or at a rotating speed of 10 000 rpm for the 260 nm- and 888 nm-thick samples. After the film deposition, the samples are cured at 150 °C for 1 h for heptane evaporation, followed by another 14 h at 75 °C for effective cross-linking. The entire film deposition and the curing processes are carried out in a clean room to avoid sample contamination. The film thickness is measured using a new distance sensor as described in ref 29.

The PDMS-coated glass plate is transferred into a closed AFM fluid cell for the AFM measurement. Before each measurement, the cell is thoroughly cleaned following the same procedure as described in ref 30. Decane (with a viscosity of 0.84 cP) is used as the working fluid, as it has stable wetting properties to the glass needle and PDMS films. The use of decane (as an organic solvent) also avoids AFM complications owing to unwanted charge interactions between the needle tip and the PDMS film. A sufficient amount of decane is filled into the fluid cell to cover the top surface of the PDMS film. Redundant decane over the PDMS surface is pipetted out to keep a thin liquid layer (30−70 μm) above the film surface. The entire fluid cell is sealed using a flexible rubber diaphragm to minimize the evaporation of the fluid during the experiment.

AFM Operation. In the experiment, an AFM (MFP-3D, Asylum Research Inc.) is used for the mechanical measurement. The AFM is operated under two modes with the control software provided by the manufacturer. The thermal power spectral density mode is used to measure the power spectrum $|z(\omega)|^2$ of vertical deflections of the cantilever. Under this mode, the cantilever is positioned stationarily, and $|z(\omega)|^2$ is measured to find the mechanical resonance of the modified cantilever and calibrate its in situ spring constant k_c (see Figures S1 and S2).[30,31]

The other mode is the FM mode, in which the resonant frequency ω'_0 and damping coefficient ξ' are measured simultaneously at a sampling rate of 2 kHz, as the fiber moves downward approaching the film surface. The z-axis piezo of the AFM is used to control the movement of the fiber at a constant speed u in the range 0.1−1 μm/s with a travel distance of s up to 26 μm. To avoid direct contact and damaging the PDMS surface by the hard press of the needle tip, the cantilever is set to automatically retreat from the PDMS surface once the driving voltage V_0 reaches a chosen set point value during the AFM measurement. More details on how to determine the contact point D = 0 in the experiment are given in the Supporting Information. All AFM experiments are conducted inside of an acoustic isolation hood (BCH-45, Asylum Research Inc.) at 24 ± 0.5 °C.

Working Principle. When an external force $f_e = F_0 \cos(\omega t)$ is applied to the cantilever, where F_0 is the amplitude and ω is the angular frequency of the driving force, the glass fiber is forced to oscillate vertically at a steady state $z(t) = Z_0 \cos(\omega t + \varphi)$, where Z_0 is the oscillation amplitude and φ is the phase delay. When the fiber tip is close to the surface of the film, as sketched in the inset of Figure 1a, the motion of the tip creates an oscillatory draining flow inward and outward in the gap region of distance D. This draining flow generates a hydrodynamic compressive force, $f_h(D)$, to the lower surface of the gap, causing deformations of the film. The lateral extension of the flow in the gap region is on the order of[32] $(2RD)^{1/2}$. Similarly, the vertical impact region in the film is also on the order of[17] $(2RD)^{1/2}$.

In the experiment, we use AFM to measure the vertical displacement $z(t)$ of the needle ($\equiv$vertical deflection of the AFM cantilever), which is well-described by an underdamped harmonic oscillator equation[30]

$$m\ddot{z} + \xi\dot{z} + k_c z = F_0 \cos(\omega t) - f_h(D) \tag{1}$$

where m is the effective mass of the modified cantilever, $\xi\dot{z}(t)$ is the drag force with ξ being the friction coefficient of the fiber, and $k_c z$ is the elastic restoring force because of the bending of the cantilever, with k_c being its spring constant. The last term in eq 1 is the hydrodynamic force, and the "−" sign indicates that $-f_h(D)$ is the reaction force acting on the fiber owing to the deformations of the film. For a small oscillation $z(t)$, one has $f_h(D) = K^*(D)z$, where $K^*(D) \equiv K'(D) + iK''(D)$ is the complex dynamic response function, containing information on the elastic and viscous moduli of the film.[13,17]

Equation 1 presents the solution

$$Z_0(\omega) = \frac{F_0/m}{\sqrt{(\omega_0'^2 - \omega^2)^2 + (\omega\xi'/m)^2}} \tag{2}$$

where the new resonant frequency $\omega'_0 = (\omega_0^2 + K'/m)^{1/2}$ and damping $\xi' = \xi + K''/\omega'_0$ contain the quantities of interest K' and K'', respectively. Here, $\omega_0 = (k_c/m)^{1/2}$ is the original resonant frequency of

the cantilever in the absence of the film response. In FM-AFM, the driving frequency ω is continuously adjusted via a phase-lock loop to keep the modified cantilever at the resonance $\omega = \omega'_0$. In this case, eq 2 can be simplified, and we have $\xi' = F_0/Z_0\omega'_0$. In the meantime, the amplitude F_0 is adjusted to keep the oscillation amplitude Z_0 at a constant set point (typically 1–2 nm). Instead of measuring Z_0 and φ as in the traditional AC response experiment, here we measure the decoupled ω'_0 and ξ' (via F_0) using FM-AFM, from which we obtain the complex response function $K^*(D)$ of the thin film

$$K'(D) = k_c\left\{\left[\frac{\omega'_0(D)}{\omega_0(D)}\right]^2 - 1\right\} \tag{3}$$

and

$$K''(D) = \omega'_0(D)[\xi'(D) - \xi(D)] \tag{4}$$

where k_c, $\xi(D)$, and $\omega_0(D)$ are the resonant parameters of the cantilever without the film response.[31,33,34] They can be independently measured from the power spectrum $|z(\omega)|^2$ of vertical deflections of the cantilever (see Supporting Information for more details).

■ RESULTS AND DISCUSSION

We now present the experimental results, which verify the method and illustrate its applications. Figure 2a shows the
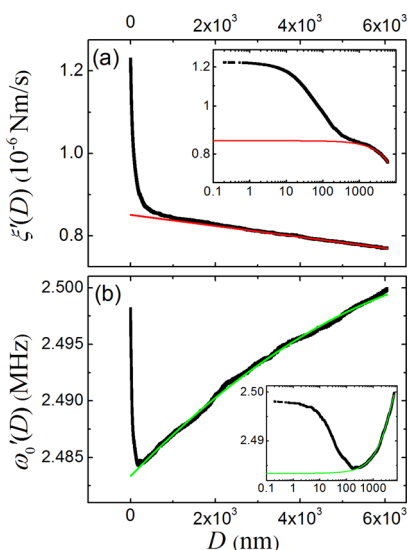
Figure 2. Measured (a) damping coefficient $\xi'(D)$ (black solid lines) and (b) resonant frequency $\omega'_0(D)$ (black solid lines) as a function of tip−sample distance D. The measurement is taken for a PDMS film with thickness $\tau = 440$ nm. The red and green lines show the fits to the data points with large values of D, which represent, respectively, the original damping coefficient $\xi(D)$ and resonant frequency $\omega_0(D)$ in the absence of the film response (see the text for more details). The insets show the same data in the linear-log plots.

measured damping coefficient $\xi'(D)$ as a function of tip−sample distance D. The measurement is taken when the long needle is partially immersed in decane and is placed near a PDMS film with thickness $\tau = 440$ nm. As the needle tip approaches the film surface, the measured $\xi'(D)$ first increases linearly with decreasing D for large values of D ($\gtrsim 1$ μm), followed by a sharp rise for small values of D (< 1 μm). The inset of Figure 2a shows the rise in the measured $\xi'(D)$ for small values of D more clearly, which is caused by the extra hydrodynamic damping resulting from the lower PDMS film. The red line is a linear fit to the data points with large values of D in the range of 2−6 μm. This linear increase in damping with

decreasing D is caused by the hydrodynamic drag of the bulk fluid acting on the thin fiber, which is approximately proportional to the fiber immersion length $h = h_0 - D$, where h_0 is the thickness of the liquid film above the PDMS surface (see eq S5). As D decreases, h increases and so does the damping coefficient $\xi(D)$ without the film response (red line).

Figure 2b shows the measured resonant frequency $\omega'_0(D)$ as a function of tip−sample distance D. For large values of D ($\gtrsim 1$ μm), the measured $\omega'_0(D)$ decreases with decreasing D, reaching a minimum value at $D \simeq 200$ nm, and then sharply increases with further decrease in D. The inset of Figure 2b more clearly shows the rise in the measured $\omega'_0(D)$ for small values of D. Again, this sharp rise is caused by the extra hydrodynamic response $K^*(D)$ of the lower PDMS film. For an oscillating fiber, there is a thin layer of fluid near its surface, which moves together with the fiber and gives rise to an added mass Δm.[35] This added mass is proportional to the fiber immersion length, $h = h_0 - D$, and changes the resonant frequency from $\omega_0 = (k_c/m_0)^{1/2}$ (in air) to $\omega_0(D) = [k_c/(m_0 + \Delta m)]^{1/2} \simeq \omega_0/(c - eD)^{1/2}$ (see eq S7), which decreases with decreasing D. The green line is a fit of the equation, $\omega_0(D) = \omega_0/(c - eD)^{1/2}$, to the data points with large values of D in the range of 1−6 μm. Here, c and e are the two adjustable parameters, with which we obtain a nice fit.

With the measured $\xi'(D)$ and $\omega'_0(D)$ and the fitted functions of $\xi(D)$ (red line) and $\omega_0(D)$ (green line) as shown in Figure 2, we now can use eqs 3 and 4 to subtract the background contribution from the bulk fluid and obtain the response function $K^*(D)$ of the PDMS film. Figure 3 shows the
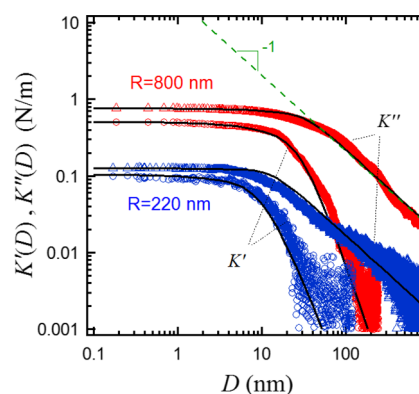
Figure 3. Measured real part $K'(D)$ (circles) and imaginary part $K''(D)$ (triangles) of the response function $K^*(D)$ as a function of tip−sample distance D for a PDMS film with thickness $\tau = 440$ nm. The measurements are taken using two different needle probes with tip radii $R = 800$ nm (red symbols) and $R = 220$ nm (blue symbols), respectively. The green dashed line shows the Reynolds damping $K''(D) = 6\pi\eta_0\omega R^2/D$ for a rigid surface. The black solid lines show the fits of the numerically calculated eq 5 to the experimental data (see text for more details).

measured real part $K'(D)$ (circles) and imaginary part $K''(D)$ (triangles) of $K^*(D)$ for a PDMS film with thickness $\tau = 440$ nm. Two different needle probes are used in the experiment; one has the tip radius $R = 800$ nm (red symbols) and the other has $R = 220$ nm (blue symbols). For the measurements with $R = 800$ nm, there is a cut-off distance D_c ($\simeq 90$ nm), beyond which the flow pressure is too small to effectively deform the PDMS surface and give rise to a measurable $K'(D)$. In this viscous regime ($D \gtrsim D_c$), the response function $K^*(D)$ is dominated by the viscous damping term $K''(D)$. For $D < D_c$,

the real part of the response $K'(D)$ increases with decreasing D and has a large slope. Eventually, the values of $K'(D)$ and $K''(D)$ both saturate at the same order of magnitude when the needle tip is a few nanometers above the PDMS surface. This is the "elastic regime," in which the fluid is no longer expelled from the gap between the two surfaces. Instead, the PDMS film deforms under the viscous pressure and accommodates most of the tip oscillations.

Because of the fluid layer in the gap region, the needle tip is not in direct contact with the PDMS surface even at the closest position to the PDMS film. As shown in eq 5 below, the hydrodynamic response function $K^*(D)$ is proportional to R^2 in the leading order. This explains why the measured values of $K'(D)$ and $K''(D)$ by a smaller probe with $R = 220$ nm are approximately 1 order of magnitude smaller than those measured by a larger probe with $R = 800$ nm. Nonetheless, we are still able to detect the film response using FM-AFM with a long-needle probe.

Figure 4 shows a comparison of the measured response function $K^*(D)$ between two PDMS films with thickness $\tau =$
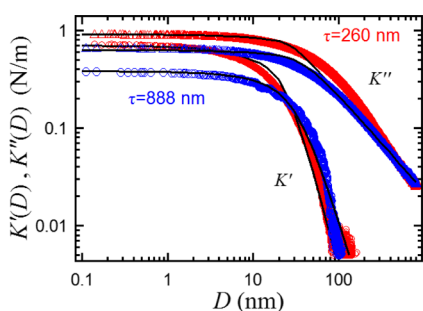

Figure 4. Measured real part $K'(D)$ (circles) and imaginary part $K''(D)$ (triangles) of the response function $K^*(D)$ as a function of tip−sample distance D. The measurements are taken using the same long-needle probe with tip radius $R = 800$ nm for PDMS films with two different values of thickness $\tau = 260$ nm (red symbols) and 888 nm (blue symbols). The black solid lines show the fits of the numerically calculated eq 5 to the experimental data (see text for more details).

260 nm (red symbols) and 888 nm (blue symbols). The data are obtained using the same long-needle probe with tip radius $R = 800$ nm. The measured $K''(D)$ curves for the PDMS films with different τ values have a similar behavior in the viscous regime ($D \gtrsim D_c$). However, in the elastic regime, both $K'(D)$ and $K''(D)$ saturate at a value that increases with reducing film thickness. This behavior is caused by the effect of the rigid glass substrate, which cannot be neglected when the film thickness τ becomes comparable to or smaller than the tip radius R. To obtain the correct value of the mechanical properties of a thin film, it is important to take the effect of substrates into account.[13]

If the film surface is perfectly rigid as the fiber probe, one has $K' = 0$ and $K''(D) = 6\pi\eta_0\omega R^2/D$,[13,36] with η_0 being the fluid viscosity. This is the Reynolds damping force between a rigid sphere and a rigid plane, which diverges as $1/D$, as indicated by the green dashed line in Figure 3. The fact that all measured $K''(D)$ curves in Figures 3 and 4 do not go as $1/D$ for small values of D but saturate at a constant value, indicating that the PDMS film is not rigid. In a previous study on PDMS films made by the same curing agent and a similar recipe,[17] it was found that the PDMS film in the aqueous glycerol solution

behaves like a pure elastic film and that the measured $K'(D)$ is larger than $K''(D)$ when D becomes smaller than D_c for sufficiently thick films with $\tau \gtrsim (2RD_c)^{1/2}$.[13] Such a crossover for $K'(D)$ from being smaller than $K''(D)$ at large values of D to becoming larger than $K''(D)$ at smaller values of D is not observed for the similar PDMS films in decane. It will be shown below that the PDMS films in decane become viscoelastic. Because decane is a good solvent for PDMS, it may enter the PDMS network and cause swelling of the films.[37]

To characterize the viscoelastic properties of the PDMS film, we use the linear response theory of the EHD, which predicted that the response function $K^*(D)$ has the scaling form[13,17]

$$K^*(D) = \mathrm{i}\frac{6\pi\eta_0\omega R^2}{D}\tilde{p}^*\left(\frac{D}{D_c}\right) \tag{5}$$

where $\tilde{p}^*(D/D_c)$ is a dimensionless complex correction function owing to the film compliance and $D_c = 8R[(1 - \nu^2)\eta_0\omega/E]^{2/3}$ is a characteristic cut-off distance, which contains information on the mechanical properties of the film, such as its Young's modulus E and Poisson ratio ν. Although under certain limiting conditions, one can obtain the analytical expressions of $\tilde{p}^*$ and D_c,[13] numerical calculations are needed in general to compare the theory with the experimental data (see section SVI for more details).

In the original EHD theory,[13] only the elastic deformation of the film was considered. For a viscoelastic film, one needs to extend the EHD theory by introducing a complex Young modulus $E^* = E + iE''$, where the imaginary component E'' is related to the viscosity η of the film via the equation $E'' = 2(1 + \nu)\omega'_0\eta$. In solving the mechanical response equation of the polymer film to the hydrodynamic pressure generated by the oscillatory draining flow in the gap region, a boundary condition is imposed that the polymer film is firmly attached to the substrate, so that a nonslip boundary condition is applied to this interface. As a result, the material parameters of both the polymer film and substrate are needed to obtain the response function $K^*(D)$ of the polymer film (see section SVI for more details).

The black solid lines in Figures 3 and 4 show the fits of the numerically calculated eq 5 to the experimental data with different values of τ and R. Here, we assume the PDMS film to be incompressible and thus choose $\nu = 1/2$. There are two free adjustable parameters, E and E'' (or E''/E), which are chosen to best fit the data. It is seen that all data are well-described by eq 5 over 4 decades of variations in distance D. The final fitting results are given in Table 1. The fitted values of E for different values of τ and R are in good agreement with each other. Furthermore, the obtained mean value $\langle E \rangle \simeq 0.6$ MPa agrees with the previous results obtained using probes of large sizes, such as the millimeter-sized surface force apparatus[17] and the

Table 1. Fitted Values of the Young's Modulus E, Viscoelastic Ratio E''/E, and Viscosity η for the PDMS Films with Different Values of Film Thickness τ and Tip Radius R[a]

τ (nm)	R (nm)	E (kPa)	E''/E	η (mPa·s)
260	800	585 ± 17	0.15	11.7 ± 2.4
440	220	600 ± 18	0.45	41.0 ± 4.1
440	800	615 ± 18	0.43	35.3 ± 3.5
888	800	605 ± 18	0.69	55.7 ± 5.6

[a]The error bars indicate the fitting uncertainties.

centimeter-sized indenter.[37] This agreement suggests that the reticulation network of the PDMS films does not change much with their thickness nor with the proximity to the glass substrate. It also demonstrates the robustness and effectiveness of the long-needle FM-AFM in the absolute measurement of the Young's modulus E, without a need for calibration against a material of known modulus.

For a thin soft film whose thickness τ is not significantly larger than the vertical impact range $(2RD_c)^{1/2}$ in the film, the underlying substrate will support a fraction of the (oscillatory) hydrodynamic stress. This explains why the measured response functions, $K'(D)$ and $K''(D)$, as shown in Figure 4 vary with τ. However, because the Young's modulus E is an intrinsic property of the film, it should not change with τ. It is seen from Table 1 that the obtained values of E for the PDMS films with different values of τ indeed remain unchanged (within the experimental uncertainties). Our results thus confirm that the modified elastohydrodynamic theory used here can properly take account of the contributions from the supporting substrate, so that the Young's modulus E of the film can be accurately extracted from the measured $K'(D)$ and $K''(D)$.

Another important property of the PDMS films is their loss modulus E'' at the resonant frequency $f'_0 = \omega'_0/2\pi \sim 350$ kHz. First, in comparison with the elastic modulus E, we find that the fitted values of E'' are always smaller than E, and the resultant ratios E''/E lie in the range measured by other means in the same frequency range.[38] Second, unlike the Young's modulus E, the effective viscosity, $\eta = E''/2(1+\nu)\omega'_0$, of the PDMS films is found to increase with the sample thickness. At the present, we do not fully understand this thickness dependence. Because consistent values of η are obtained when two needles of different tip radii are used (see Table 1), it is unlikely to be caused by the molecular rearrangements of the polymer chains inside of the network. One possible cause is the poroelasticity of the PDMS film, resulting from the motion of the solvent in the PDMS matrix under the applied pressure gradient, which may depend on the film thickness.[39]

Finally, we make an estimate on how much the PDMS film deforms during the noncontact tapping. As mentioned above, the vertical impact range in the film is on the order of $(2RD)^{1/2}$. This impact depth is about 400 nm for a gap distance $D \simeq D_c \simeq 90$ nm and a tip radius $R = 800$ nm, which are typical values used in the experiment. The actual deformation of the film is given by $\delta = f_h/k_s$, where $f_h(D) \simeq K''(D)Z_0 \simeq (6\pi\eta_0\omega R^2/D)Z_0$ is the hydrodynamic force acting on the film surface over an area $2\pi RD$ and $k_s \simeq \pi(2RD)^{1/2}E/(1-\nu^2)$ is the stiffness of the polymer film.[17] For large surface separations with $D \gtrsim D_c$, the maximal value of δ is $\delta_m \simeq 0.5$ nm at $D = D_c$. This small value of δ_m confirms that the hydrodynamic force $f_h(D)$ at distances $D > D_c$ is too weak to deform the polymer film significantly, so that $K''(D) \sim 1/D$ remains the same as that for a rigid surface. For small surface separations with $D < D_c$, the film surface oscillates together with the needle tip, so that the film deformation δ becomes equal to the oscillation amplitude Z_0, which is in the range of 1–2 nm.

SUMMARY AND CONCLUSIONS

We have carried out a systematic study of the viscoelastic property of thin PDMS films in a liquid medium using the newly developed long-needle AFM under the FM mode. The long-needle FM-AFM has several features particularly useful for the investigation intended here: (i) By using the fiber tip to touch the liquid and keeping the major part of the cantilever in

air, the viscous drag force acting on the fiber is greatly reduced. (ii) Being operated at a resonant state, the long needle amplifies the oscillation signal and thus can accurately detect minute changes in the damping ξ' and resonant frequency ω'_0 caused by the dynamic response of the film at a distance. This superior sensitivity is essential for the study of soft materials (such as live cells) and nanometer-sized thin films, which typically have a very weak mechanical response to the applied oscillations. (iii) The capability of detecting weak signals with light tapping and at a distance from the film surface together with the recently developed linear response theory of EHD under the sphere–plane geometry allow us to obtain quantitative information on the viscoelastic properties of the film. (iv) Finally, the radial extension of the flow in the gap region, as sketched in the inset of Figure 1a, and its vertical impact range are on the order of[17,32] $(2RD)^{1/2}$. This probe range can be even smaller than the tip radius R when working at a close distance $(D < R)$, which allows us to investigate the mechanical properties of thin films in the nanometer range. The experiment clearly demonstrates that the long-needle FM-AFM can accurately measure the viscoelastic property of the thin PDMS films at a nanoscale distance without any direct contact. The general methodology presented here can be further extended to nanomechanical detection and imaging of other soft interfaces and membranes of live cells in a liquid environment.

■ ASSOCIATED CONTENT

⑤ Supporting Information

The Supporting Information is available free of charge on the ACS Publications website at DOI: 10.1021/acs.langmuir.6b04066.

> Details on the fabrication of the long-needle probe, measurement of the power spectrum of the long-needle probe, calibration of the driving force, determination of contact point, measured damping coefficient and added mass of the long-needle probe, and numerical calculation of the correction function $\tilde{p}*(D/D_c)$ (PDF)

■ AUTHOR INFORMATION

Corresponding Author

*E-mail: penger@ust.hk.

ORCID 🄍

Dongshi Guan: 0000-0002-4433-3662

Notes

The authors declare no competing financial interest.

■ ACKNOWLEDGMENTS

■ REFERENCES

(1) Janmey, P. A.; McCulloch, C. A. Cell mechanics: Integrating cell responses to mechanical stimuli. *Annu. Rev. Biomed. Eng.* **2007**, 9, 1–34.

(2) Moeendarbary, E.; Valon, L.; Fritzsche, M.; Harris, A. R.; Moulding, D. A.; Thrasher, A. J.; Stride, E.; Mahadevan, L.; Charras, G. T. The cytoplasm of living cells behaves as a poroelastic material. *Nat. Mater.* **2013**, 12, 253–261.

(3) Vogel, V.; Sheetz, M. Local force and geometry sensing regulate cell functions. *Nat. Rev. Mol. Cell Biol.* **2006**, *7*, 265−275.

(4) Walczyk, W.; Schönherr, H. Characterization of the interaction between AFM tips and surface nanobubbles. *Langmuir* **2014**, *30*, 7112−7126.

(5) Lohse, D.; Zhang, X. Surface nanobubbles and nanodroplets. *Rev. Mod. Phys.* **2015**, *87*, 981.

(6) Stafford, C. M.; Harrison, C.; Beers, K. L.; Karim, A.; Amis, E. J.; VanLandingham, M. R.; Kim, H.-C.; Volksen, W.; Miller, R. D.; Simonyi, E. E. A buckling-based metrology for measuring the elastic moduli of polymeric thin films. *Nat. Mater.* **2004**, *3*, 545−550.

(7) Johnson, K. L. *Contact Mechanics*; Cambridge University Press, 1985.

(8) Popov, V. L. *Contact Mechanics and Friction—Physical Principles and Applications*; Springer-Verlag, 2010.

(9) Shull, K. R. Contact mechanics and the adhesion of soft solids. *Mater. Sci. Eng., R* **2002**, *36*, 1−45.

(10) Barthel, E.; Perriot, A. Adhesive contact to a coated elastic substrate. *J. Phys. D: Appl. Phys.* **2007**, *40*, 1059.

(11) Chu, Y.-S.; Dufour, S.; Thiery, J. P.; Perez, E.; Pincet, F. Johnson−Kendall−Roberts theory applied to living cells. *Phys. Rev. Lett.* **2005**, *94*, 028102.

(12) Lauga, E.; Brenner, M. P. Dynamic mechanisms for apparent slip on hydrophobic surfaces. *Phys. Rev. E: Stat., Nonlinear, Soft Matter Phys.* **2004**, *70*, 026311.

(13) Leroy, S.; Charlaix, E. Hydrodynamic interactions for the measurement of thin film elastic properties. *J. Fluid Mech.* **2011**, *674*, 389−407.

(14) Kaveh, F.; Ally, J.; Kappl, M.; Butt, H.-J. Hydrodynamic Force between a Sphere and a Soft, Elastic Surface. *Langmuir* **2014**, *30*, 11619−11624.

(15) Roters, A.; Gelbert, M.; Schimmel, M.; Rühe, J.; Johannsmann, D. Static and dynamic profiles of tethered polymer layers probed by analyzing the noise of an atomic force microscope. *Phys. Rev. E: Stat. Phys., Plasmas, Fluids, Relat. Interdiscip. Top.* **1997**, *56*, 3256−3264.

(16) DeNolf, G. C.; Haack, L.; Holubka, J.; Straccia, A.; Blohowiak, K.; Broadbent, C.; Shull, K. R. High Frequency Rheometry of Viscoelastic Coatings with the Quartz Crystal Microbalance. *Langmuir* **2011**, *27*, 9873−9879.

(17) Leroy, S.; Steinberger, A.; Cottin-Bizonne, C.; Restagno, F.; Léger, L.; Charlaix, É. Hydrodynamic Interaction between a Spherical Particle and an Elastic Surface: A Gentle Probe for Soft Thin Films. *Phys. Rev. Lett.* **2012**, *108*, 264501.

(18) Walczyk, W.; Hain, N.; Schönherr, H. Hydrodynamic effects of the tip movement on surface nanobubbles: A combined tapping mode, lift mode and force volume mode AFM study. *Soft Matter* **2014**, *10*, 5945−5954.

(19) Vinogradova, O. I.; Butt, H.-J.; Yakubov, G. E.; Feuillebois, F. Dynamic effects on force measurements. I. Viscous drag on the atomic force microscope cantilever. *Rev. Sci. Instrum.* **2001**, *72*, 2330−2339.

(20) Gavara, N.; Chadwick, R. S. Noncontact microrheology at acoustic frequencies using frequency-modulated atomic force microscopy. *Nat. Methods* **2010**, *7*, 650−654.

(21) Fong, K. Y.; Poot, M.; Tang, H. X. Nano-optomechanical resonators in microfluidics. *Nano Lett.* **2015**, *15*, 6116−6120.

(22) Hansma, P. K.; Cleveland, J. P.; Radmacher, M.; Walters, D. A.; Hillner, P. E.; Bezanilla, M.; Fritz, M.; Vie, D.; Hansma, H. G.; Prater, C. B.; Massie, J.; Fukunaga, L.; Gurley, J.; Elings, V. Tapping mode atomic force microscopy in liquids. *Appl. Phys. Lett.* **1994**, *64*, 1738−1740.

(23) Walters, D. A.; Cleveland, J. P.; Thomson, N. H.; Hansma, P. K.; Wendman, M. A.; Gurley, G.; Elings, V. Short cantilevers for atomic force microscopy. *Rev. Sci. Instrum.* **1996**, *67*, 3583−3590.

(24) Guan, D.; Wang, Y. J.; Charlaix, E.; Tong, P. Asymmetric and speed-dependent capillary force hysteresis and relaxation of a suddenly stopped moving contact line. *Phys. Rev. Lett.* **2016**, *116*, 066102.

(25) Guan, D.; Wang, Y. J.; Charlaix, E.; Tong, P. Simultaneous observation of asymmetric speed-dependent capillary force hysteresis and slow relaxation of a suddenly stopped moving contact line. *Phys. Rev. E* **2016**, *94*, 042802.

(26) Fukuma, T.; Kilpatrick, J. I.; Jarvis, S. P. Phase modulation atomic force microscope with true atomic resolution. *Rev. Sci. Instrum.* **2006**, *77*, 123703.

(27) Kobayashi, K.; Yamada, H.; Matsushige, K. Frequency noise in frequency modulation atomic force microscopy. *Rev. Sci. Instrum.* **2009**, *80*, 043708.

(28) Minary-Jolandan, M.; Tajik, A.; Wang, N.; Yu, M.-F. Intrinsically high-Q dynamic AFM imaging in liquid with a significantly extended needle tip. *Nanotechnology* **2012**, *23*, 235704.

(29) Villey, R.; Piednoir, A.; Sharma, P.; Cottin-Bizonne, C.; Cross, B.; Phaner-Goutorbe, M.; Charlaix, É. Capacitive detection of buried interfaces by a dynamic surface force apparatus. *Rev. Sci. Instrum.* **2013**, *84*, 2292−2297.

(30) Xiong, X.; Guo, S.; Xu, Z.; Sheng, P.; Tong, P. Development of an atomic-force-microscope-based hanging-fiber rheometer for interfacial microrheology. *Phys. Rev. E: Stat., Nonlinear, Soft Matter Phys.* **2009**, *80*, 061604.

(31) Guan, D.; Hang, Z. H.; Marcet, Z.; Liu, H.; Kravchenko, I. I.; Chan, C. T.; Chan, H. B.; Tong, P. Direct measurement of optical force induced by near-field plasmonic cavity using dynamic mode AFM. *Sci. Rep.* **2015**, *5*, 16216.

(32) Chan, D. Y. C.; Horn, R. G. The drainage of thin liquid films between solid surfaces. *J. Chem. Phys.* **1985**, *83*, 5311−5324.

(33) Benmouna, F.; Johannsmann, D. Hydrodynamic interaction of AFM cantilevers with solid walls: An investigation based on AFM noise analysis. *Eur. Phys. J. E: Soft Matter Biol. Phys.* **2002**, *9*, 435−441.

(34) Guo, S.; Gao, M.; Xiong, X.; Wang, Y. J.; Wang, X.; Sheng, P.; Tong, P. Direct measurement of friction of a fluctuating contact line. *Phys. Rev. Lett.* **2013**, *111*, 026101.

(35) Landau, L. D.; Lifshitz, E. M. *Fluid Mechanics*, 2nd ed.; Butterworth-Heinemann, 1986.

(36) Brenner, H. The slow motion of a sphere through a viscous fluid towards a plane surface. *Chem. Eng. Sci.* **1961**, *16*, 242−251.

(37) Hu, Y.; Chen, X.; Whitesides, G. M.; Vlassak, J. J.; Suo, Z. Indentation of polydimethylsiloxane submerged in organic solvents. *J. Mater. Res.* **2011**, *26*, 785−795.

(38) Pottier, B.; Ducouret, G.; Frétigny, C.; Lequeux, F.; Talini, L. High bandwidth linear viscoelastic properties of complex fluids from the measurement of their free surface fluctuations. *Soft Matter* **2011**, *7*, 7843−7850.

(39) Hu, Y.; Suo, Z. Viscoelasticity and poroelasticity in elastomeric gels. *Acta Mech. Solida Sin.* **2012**, *25*, 441−458.